EUROPEAN FUSION DEVELOPMENT AGREEMENT

EFDA–JET–PR(04)-39

G. Rewoldt, R. V. Budny, W. M. Tang and JET EFDA Contributors

Multispecies Density and Temperature Gradient Dependence of Quasilinear Particle and Energy Fluxes

Multispecies Density and Temperature Gradient Dependence of Quasilinear Particle and Energy Fluxes

G. Rewoldt, R. V. Budny, W. M. Tang and JET EFDA Contributors*

Princeton Plasma Physics Laboratory, Princeton University, Princeton, New Jersey 08543-0451
** See annex of J. Pamela et al, "Overview of Recent JET Results and Future Perspectives", Fusion Energy 2002 (Proc.19 th IAEA Fusion Energy Conference, Lyon (2002)).*

Preprint of Paper to be submitted for publication in
Physics of Plasmas

ABSTRACT.

The variations of the normalised quasilinear particle and energy fluxes with artificial changes in the density and temperature gradients, as well as the variations of the linear growth rates and real frequencies, for ion temperature gradient and trapped-electron modes, are calculated. The quasilinear fluxes are normalised to the total energy flux, summed over all species. Here, realistic cases for tokamaks and spherical torii are considered which have two impurity species, specifically cases for the Joint European Torus (JET). For situations where there are substantial changes in the normalised fluxes, the "diffusive approximation," in which the normalised fluxes are taken to be linear in the gradients, is seen to be inaccurate. In the case of artificial changes in density or temperature gradients, changes in the fluxes of different species ("off-diagonal") generally are significant, or even dominant, compared to those for the same species ("diagonal").

1. INTRODUCTION

The FULL code1,2 can calculate the linear eigenfrequencies and eigenfunctions of high-*n* instabilities in tokamaks and spherical torii and other devices, using the ballooning formalism so that the calculation is radially local. It can also calculate the corresponding quasilinear particle and energy fluxes for each species included in the calculation, using the converged eigenfrequency-eigenfunction results, and the fluxes are proportional to the square of the saturation level of the perturbed electrostatic potential for the instability. In the linear and quasilinear limit, this saturation level is unknown, but if ratios of quasilinear fluxes are taken, the unknown saturation level divides out. In the present work, the dependence of the quasilinear particle flux Γ_j and total energy flux Q_j (including any convective part) for species j on the density gradient dn_j/dr and the temperature gradient dT_j/dr, both of the same species ("diagonal") and of different species ("off-diagonal"), will be examined for two experimentally-realistic cases.

The particle fluxes will be normalized to $Q_{tot} = T_j$ and the energy fluxes to Q_{tot}, where $Q_{tot} \equiv \Sigma_j Q_j$, and the sum is over the electrons and all of the ion species. The resulting dimensionless normalized fluxes, independent of the unknown nonlinear saturation level, will be examined for their variation with the density and temperature gradients of each of the species from their experimental values.

Among other things, this variation will allow us to examine the accuracy of the "diffusive approximation," in which the flux is considered to be linear in the corresponding gradient. This diffusive approximation means, in the most simplified case with a single (density) gradient and a single (particle) flux, that $\Gamma(dn/dr) = nV - D(dn/dr)$, where V and D are considered to be independent of (dn/dr). This expression can be thought of as a power series expansion of Γ (dn/dr) in dn/dr, truncated after the first two terms. Here, we will examine the validity of the generalization of this approximation, to both density and temperature gradients and to multiple species, for the normalized quasilinear flux results, which are general nonlinear functions of all of the gradients.

There is already a large literature on plasma transport from micro-instabilities. For example, purely analytic results for fluxes due to ion temperature gradient and trapped electron modes in a

pure plasma are obtained in Ref.3, making various approximations including the mixing-length saturation level approximation. These results are used along with those for other instabilities in the so-called Multi-Mode Model, [4,5] which is used in predictive transport codes such as BALDUR [6]. In addition, there are results from nonlinear simulation codes such as GS2 [7,8] and GYRO [9] and GTC [10], which normally express the transport results, for instance for the ion energy transport, in terms of a transport coefficient $\chi_i \equiv -Q_i/(n_i\, dT_i/dr)$ instead of in terms of the flux Q_i itself. Nonlinear results of this sort from several simulation codes in the Cyclone project comparison for χ_i as a function of dT_i/dr are presented [11], for a pure plasma, with other approximations. Some limited results have previously been presented, for instance for the electron particle flux as a function of the electron density gradient from nonlinear GS2 calculations [12]. However, none of this previous work examines the explicit temperature and density gradient dependence of the particle and energy fluxes for experimentally-realistic multispecies cases, to assess the degree of validity of the diffusive approximation, as is done here within the limits of a quasilinear calculation. While this would be possible in principle using a nonlinear simulation code, nonlinear simulation runs for many gradient scans would be extremely expensive computationally, at the present time. It should be noted that the Ficksian proportionality between the gradients and the fluxes exists for collisional transport [13]. However, from theoretical considerations, there is no surprise that the diffusive approximation has severe limitations in turbulence-driven transport [14]. For instance, a weak-turbulence theory of the toroidal collisionless trapped-electron mode [15] predicts that the anomalous fluxes are strongly nonlinear functions of the thermodynamic forces (gradients).

The experimental cases considered are described in Sec.2, the different unstable modes and the roots of the eigenmode equation are discussed in Sec.3, and the constraints on the input gradients for the calculation and on the resultant fluxes are explained in Sec. 4. Then, the results of the separate artificial variation of each density and temperature gradient are described in Sec.5. Limited comparisons of the calculated normalized fluxes with the corresponding experimentally-derived normalized fluxes are made in Sec.6, and general trends and conclusions.

2. CASES

We will consider a case for the Joint European Torus [16] (JET) tokamak and a case for the National Spherical Torus Experiment (NSTX) [17] spherical torus. JET and NSTX discharges of the types considered here are discussed from an experimental point of view [18,19], respectively. The JET case corresponds to JET Pulse No: 53030 at t = 21.5 s, and the NSTX case corresponds to discharge 108213 at t = 0.320s, but using the neon density profile measured for the nominally identical discharge 108216 at that time. JET Pulse No: 53030 is an ELMy H-mode plasma with argon seeding, with global parameters R = 2.9m, a = 0.9m, I_p = 2.5MA, B_Z = 2.5T, P_{NB} = 12.3MW, $T_i(0) = T_C(0)$ = 2.6keV, $T_e(0)$ = 2.9keV, and $n_e(0) = 1.1 \times 10^{20}$ m^{-3}. NSTX discharge 108213 is an L-mode plasma without neon injection and NSTX discharge 108216 is an L-mode plasma with neon injection, both with global parameters R = 0.87m, a = 0.65 m, I_p = 1.0MA, B_Z = 0.44T, P_{NB} = 1.6MW,

$T_i(0) = T_C(0) = 1.6$keV, $T_e(0) = 1.2$keV, and $n_e(0) = 4.1\times 10^{19}$ m^{-3}. In addition to the usual electron (*e*), background thermal deuterium ion (*i*), carbon impurity (*C*, $Z_C = 6$), and hot deuterium beam (*b*) species, each of these cases includes a second heavier impurity species with a very small density fraction, argon (*Ar*, $Z_{Ar} = 18$) for the JET case and neon (*Ne*, $Z_{Ne} = 10$) for the NSTX case. We approximate the impurity species for each case as fully stripped, though this will not quite be achieved in the experiments at the radii of interest. All of the species are employed with Maxwellian equilibrium distribution functions. We choose $r/a = 0.750$ and $k_\theta\rho_i = 0.50$ for the "hybrid" root for the JET case, and we choose $r/a = 0.720$ and $k_\theta\rho_i = 0.262$ for the Ion Temperature Gradient (ITG) mode root for the NSTX case, and $r/a = 0{:}730$ and $k_\theta\rho_i = 0.248$ for the Trapped-Electron Mode (TEM) root for the NSTX case, since these values approximately maximize the linear growth rates of the instabilities considered. Note also that the values of $k_\theta\rho_i$ that maximize the linear growth rates can shift somewhat away from the fixed values used here, as the individual density and temperature gradients are artificially varied. These different roots and their relationships will be discussed in Sec.III.

The experimentally-reconstructed MagnetoHydroDynamic (MHD) equilibria for these cases are calculated numerically in flux coordinates, using the experimentally measured or calculated density and temperature profiles for each species. The MHD equilibria include finite-β effects such as the Shafranov shift, and are not up-down symmetric. The flux surface label r/a is *defined* in terms of the normalized toroidal flux, $r/a \equiv \sqrt{\Phi/\Phi_a}$, where *a* refers to the plasma boundary. Thus, *r* is only approximately a geometrical length (and constitutes a particular kind of average radius for the flux surface), but specifically refers to this function of the toroidal flux. When the density and temperature gradients of each species are artificially varied from their experimental values in the FULL code instability calculation, the MHD equilibrium is held fixed; in this sense the calculation is not self-consistent. Also, in experimental plasmas, the local value and the local gradient of a plasma parameter are highly correlated, but here we are changing only the individual gradients, in the previous artificial sense of Green and Chance [20].

The local experimental parameters for the JET case at $r/a = 0.75$ are: $n_e = 6.30 \times 10^{19}$ m^{-3}, $T_e = 1.40$keV, $T_i = 1.27$keV, $T_C = T_{Ar} = 1.27$keV, $T_b = 23.1$keV, $n_i/n_e = 0.907$, $n_C/n_e = 0.0141$, $n_{Ar}/n_e = 0.0000614$, $n_b/n_e = 0.00764$, $r_{ni}/r_{ne} = 1.12$, $r_{nC}/r_{ne} = 0.473$, $r_{nAr}/r_{ne} = 9.89$, $r_{nb}/r_{ne} = 0.575$, $\eta_e = 1.99$, $\eta_i = 3.04$, $\eta_C = 1.28$, $\eta_{Ar} = 26.7$, $\eta_b = 0.486$, and $q = 2.01$. Here, $r_{nj} \equiv -(d \ln n_j/dr)^{-1}$ and $\eta_j \equiv (d \ln T_j/dr)/(d \ln n_j/dr)$, and the other notation is standard.

The local experimental parameters for the ITG root for the NSTX case at $r/a = 0.72$ are: $n_e = 1.87 \times 10^{19}$ m^{-3}, $T_e = 0.179$keV, $T_i = 0.180$keV, $T_C = T_{Ne} = 0.180$keV, $T_b = 18.5$keV, $n_i/n_e = 0.947$, $n_C/n_e = 0.00534$, $n_{Ne}/n_e = 0.00187$, $n_b/n_e = 0.00192$, $r_{ni}/r_{ne} = 1.10$, $r_{nC}/r_{ne} = 0.403$, $r_{nNe}/r_{rne} = 0.364$, $r_{nb}/r_{ne} = 0.192$, $\eta_e = 1.91$, $\eta_i = 2.29$, $\eta_C = 0.835$, $\eta_{Ne} = 0.755$, $\eta_b = -0.169$, and $q = 2.12$. The local experimental parameters for the TEM root for the NSTX case at $r=a = 0.73$ are: $n_e = 1.82\times 10^{19}$ m^{-3}, $T_e = 0.170$keV, $T_i = 0.170$keV, $T_C/T_{Ne} = 0.170$keV, $T_b = 18.9$keV, $n_i/n_e = 0.950$, $n_C/n_e = 0.00516$, $n_{Ne}/n_e = 0.00177$, $n_b/n_e = 0.00170$, $r_{ni}/r_{ne} = 1.09$, $r_{nC}/r_{ne} = 0.503$, $r_{nNe}/r_{ne} = 0.321$, $r_{nb}/r_{ne} = 0.192$, $\eta_e = 1.92$, $\eta_i = 2.19$, $\eta_C = 1.01$, $\eta_{Ne} = 0.645$, $\eta_b = -0.178$, and $q = 2.20$.

3. MODES AND ROOTS

The linear instability calculation is performed with the FULL code in the electrostatic limit, without rotation, including collisions, for $k_\theta \rho_i \lesssim 1$, but with $n >> 1$. In this limit, there are two modes of interest: the Ion Temperature Gradient (ITG) mode and the Trapped-Electron Mode (TEM), which normally have real frequencies ω_r in the ion and the electron diamagnetic directions, respectively. Depending on the parameters, these two modes can remain as separate roots of the eigenmode equation, as happens here for the NSTX case, or can "hybridize" into a single root, as happens here for the JET case. For a hybrid root, the real frequency ω_r will normally make a transition from the electron diamagnetic direction to the ion diamagnetic direction as $k_\theta \rho_i$ increases, and the hybrid root correspondingly goes from a TEM-like regime to an ITG-like regime.

The behaviour of the roots depends strongly on the parameter $\eta_i^e \equiv (d \ln T_i/d_r)=(d \ln n_e/d_r)$. Increasing η_i^e will also normally move the real frequency from the electron diamagnetic direction to the ion diamagnetic direction; η_i^e can be changed either by varying (dT_i/d_r) or by varying $(dne=dr)$, but it will be seen that the two kinds of variation are not equivalent.

4. CONSTRAINTS

There are constraints both on the input to and on the output of the calculation. The input constraints come from the requirement of electric charge neutrality on every magnetic surface. Not only does this require that $\Sigma_j Z_j n_j = 0$ on the chosen magnetic surface for the calculation, but the radial derivative of this charge neutrality condition also imposes a condition on the density gradients of the different species. If the density gradients of all but one of the species are chosen freely, then this condition determines the value of the density gradient of the remaining species. As a matter of convention, this adjusted species is taken to be the background thermal deuterium ion species, though this is an arbitrary choice (and the results would be somewhat different with a different choice). Thus, as other species are turned on or off in the FULL code, or as the densities or density gradients of other species are changed, the density and density gradient of the background thermal deuterium ion species are adjusted to satisfy the requirements of charge neutrality and of the radial derivative of charge neutrality on the chosen magnetic surface.

There is also a constraint on the output of the calculation, in particular on the quasilinear particle fluxes. It was shown in Ref.2 that these modes satisfying the quasi-neutrality condition cause no net flux of electric charge, that is $\Sigma_j Z_j \Gamma_j = 0$, and the transport is thus automatically ambipolar. When the eigenfrequency and eigenfunction satisfy the eigenmode equation to good accuracy, this ambipolarity condition is also satisfied to good accuracy. Thus, when some parameter is changed, and the particle fluxes of the other species change correspondingly, the particle flux of one species (again, say the background thermal deuterium ion species) can be regarded as adjusting to satisfy this ambipolarity condition.

5. RESULTS

In this section we examine the effects of artificial gradient variation on the linear growth rates and real frequencies of the different modes, and on the corresponding normalized quasilinear particle and energy fluxes for the five species. There are four independent density gradients, as explained in Sec. IV, and five independent temperature gradients, which will generally be varied from zero up to twice the corresponding experimental values, so that there are nine gradients to be varied in all, and the results are shown in nine figures. There are five particle fluxes (four independent, as explained in Sec. IV), and five energy fluxes for each root, for each set of input gradients. We will vary the input gradients roughly in order from those which have the largest effect on the normalized fluxes, to those with successively smaller effects. For the JET case, there is only one "hybrid" root, and thus only one Q_{tot}, but for the NSTX case there are separate ITG and TEM roots, so we use separate Q_{tot}^{ITG} and Q_{tot}^{TEM} normalizations for them, and these can in general be different.

The sub¯gures in the left-hand column for each figure are for the JET case and those in the right-hand column are for the NSTX case. The top pair of sub figures in each figure shows the growth rate $\gamma$and the real frequency ω_r, the middle pair of sub figures shows the normalized particle fluxes $\Gamma_j T_j/Q_{tot}$, and the bottom pair of sub figures shows the normalized total energy fluxes Q_j/Q_{tot}. The growth rates are shown as solid lines and the real frequencies as dashed lines, the JET hybrid root fluxes and the NSTX ITG mode fluxes as solid lines and the NSTX TEM mode fluxes as dashed lines. The color coding is that the JET hybrid mode and the NSTX ITG mode eigenfrequencies are in black, the NSTX TEM mode eigenfrequencies are in yellow, the electron (*e*) fluxes are in magenta, the background thermal deuterium ion (*i*) fluxes are in red, the carbon (*C*) fluxes are in green, the argon (*Ar*) or neon (*Ne*) fluxes are in cyan, and the hot deuterium beam (*b*) fluxes are in blue.

A. ION TEMPERATURE GRADIENT

In Fig.1 the results of varying the background thermal deuterion ion (ion) species temperature gradients from zero to two times the experimental value for the JET case, and from zero to three times the experimental value for the NSTX case, are shown. In Fig.1(a) for the JET case, only the ITG-like range of the JET hybrid root is seen; the TEM-like range will be seen when other gradients are varied. In Fig.1(b) for the NSTX case, the NSTX TEM root has very small growth rate for the experimental parameters, but acquires a larger growth rate as the ion temperature gradient is decreased or, as will be seen, the electron density gradient is increased. Also, the NSTX ITG root growth rate increases as the ion temperature gradient increases above a threshold value. In Fig.1(c) and (d), the normalized electron particle fluxes decrease with increasing ion temperature gradient, gradually for the JET case, and gradually, then steeply after a root transition, and then gradually again for the NSTX case. The carbon particle flux decreases, for increasing ion temperature gradient above a certain value, while the argon, neon, and beam species particle fluxes are always small. The ion particle flux is positive (outward), then negative (inward), and then positive again, for both cases, with increasing ion temperature gradient, to balance the particle fluxes of the other species so as to

give zero net electric charge flux, as explained in Sec.4. Note that any change in the carbon particle flux has to be balanced by a six-times larger change in the ion particle flux to satisfy this condition, and correspondingly for the argon and neon species.

Note also that the scales on the particle flux Figs.1(c) and (d) are different from the scales for the energy flux Figs.1(e) and (f). The particle fluxes ¡j are always small compared to Q_{tot}/T_j for all species, while the largest Q_j for any species can be comparable to Q_{tot}. This will be seen to be true regardless of which gradient is being varied.

For both cases, as the ion temperature gradient is increased above a certain value, the normalized ion energy flux increases, while the normalized electron and carbon energy fluxes decrease, though more steeply for the NSTX case than for the JET case, and the normalized argon or neon and beam energy fluxes are always small. The beam particle and energy fluxes are small not only because of the small beam density fraction, but also because the beam particles interact weakly with these modes. The bounce frequencies for trapped beam particles and the transit frequencies for untrapped beam particles are large compared to the mode frequencies for all of the roots, and this causes weak interaction of these modes with the beam species.

These results for $\Gamma_j T_j/Q_{tot}$ and Q_j/Q_{tot} as functions of dT_i/dr all seem to have a sub-stantial amount of "curvature," or departure from linearity (indicating the poorness of the diffusive approximation), except when the amount of variation is small, and appear to be asymptoting to a constant value as dT_i/dr reaches its maximum value in these plots. The corresponding variation in the unnormalized fluxes Γ_j and Q_j will be modified by whatever variation comes through the Q_{tot} factor for the respective root, and that is unknown in the present calculation.

B. ELECTRON DENSITY GRADIENT

The variation with the electron density gradient is shown in Fig.2, from zero to three times the experimental value for the JET case, and from zero to two times the experimental value for the NSTX case. As dn_e/dr increases from somewhat more than the experimental value in Fig.2(a), for the JET case, the TEM-like range of the hybrid root occurs, with the real frequency making a transition into the electron diamagnetic direction. For the NSTX case in Fig.2(b), the TEM root has a very small growth rate for the experimental value of dn_e/dr, but becomes strongly unstable as the density gradient increases. The ITG root is stabilized if the electron density gradient becomes either too large or too small compared to the experimental value.

As dn_e/dr increases for the JET case in Fig.2(c), the normalized electron particle °ux increases gradually, then steeply, and then saturates. The carbon particle flux increases to a maximum, and then decreases, over the same range. To maintain ambipolarity, the ion particle flux is first positive, then negative, and then positive again. The argon and beam species fluxes are small. All of these statements hold also for the NSTX case in Fig.2(d), except that there is a transition from the ITG root to the TEM root in the progression. For the normalized energy fluxes in Fig.2(e) for the JET case, Q_i/Q_{tot} decreases and Q_e/Q_{tot} increases as $dne=dr$ increases, with near saturation at the

maximum of dn_e/dr; Q_C/Q_{tot} has a maximum near where Q_i/Q_{tot} and Q_e/Q_{tot} are changing most rapidly, which is where $!r$ has the smallest magnitude (this allows stronger interaction of the mode with the carbon species). The beam and argon fluxes are small. Again, these statements apply also for the NSTX case in Fig.2(f), but again with the ITG to TEM root transition.

Also, Γ_{Ne}^{ITG} T_{Ne}/Q_{tot}^{ITG} and Γ_C^{ITG} T_C/Q_{tot}^{ITG}, as well as Q_{Ne}/Q_{tot} and Q_C/Q_{tot}, change sub- stantially just before the ITG root goes stable with increasing dn_e/dr, but Q_{tot} would pre-sumably be getting small close to marginal stability also, so there would probably be no corresponding substantial increases in Γ_{Ne}, Γ_C, Q_{Ne}, and Q_C themselves.

C. ELECTRON TEMPERATURE GRADIENT

The effects of varying electron temperature gradient are somewhat weaker than those of varying ion temperature gradient or of varying electron density gradient for these cases, as shown in Fig.3. The JET case hybrid root is somewhat destabilized by increasing dT_e/dr, as is the NSTX case ITG root, while for the NSTX case the weak TEM root is stabilized by dT_e/dr changing too much in either direction. The changes in the normalized particle and energy fluxes for the JET case are moderate, and the temperature gradient dependence is close to being linear. However, for the corresponding NSTX case fluxes, there is still noticable "curvature." With increasing dT_e/dr, there is an increase in Q_e/Q_{tot} and a corresponding decrease in Q_i/Q_{tot} for all roots, with moderate changes for the other species.

D. CARBON DENSITY GRADIENT

Increasing carbon density gradient is stabilizing for all cases and roots here, as shown in Fig.4. The normalized carbon particle and energy fluxes increase, with a corresponding decrease in the ion particle flux, satisfying the ambipolarity condition. The effects on the fluxes of other species is moderate or small.

E. CARBON TEMPERATURE GRADIENT

Increasing carbon temperature gradient has little effect on the growth rates, as shown in Fig.5. As with the carbon density gradient, increasing carbon temperature gradient increases the normalized carbon particle and energy fluxes, with a corresponding decrease in the ion particle flux, with little change in the fluxes for the other species.

F. ARGON AND NEON DENSITY GRADIENT

The effects of varying the argon density gradient for the JET case and the neon density gradient for the NSTX case are shown in Fig.6. The density fractions n_{Ar}/n_e and n_{Ne}/n_e are small, and the effects of the density gradient variation are correspondingly weak. Increasing dn_{Ne}/dr stabilizes the already very weak TEM root for the NSTX case. The changes in the normalized fluxes $\Gamma_j T_j/Q_{tot}$ and Q_j/Q_{tot} are also very weak, except for the TEM root for the NSTX case just before the marginal

stability point, and, in this range for dn_{Ne}/dr, Q_{tot} should be going to zero, so that the corresponding unnormalized fluxes Γ_j and Q_j should also be going to zero.

G. ARGON AND NEON TEMPERATURE GRADIENT

Again, the small density fractions n_{Ar}/n_e and n_{Ne}/n_e give small or moderate changes in the eigenfrequencies and normalized fluxes when the argon and neon temperature gradients are changed, as shown in Fig.7.

H. BEAM DENSITY GRADIENT

The hot deuterium beam species density fraction n_b/n_e is also small, and the changes in the growth rates and real frequencies and the *absolute* changes in the normalized particle and energy fluxes are small for all species, as shown in Fig.8. However, the *relative* changes in the normalized beam species fluxes $\Gamma_b T_b/Q_{tot}$ and Q_b/Q_{tot} are large, of order unity, for this order unity change in dn_b/d_r. This relative change is difficult to see in Fig.8, because the absolute magnitudes of $\Gamma_b T_b/Q_{tot}$ and Q_b/Q_{tot} are so small.

I. BEAM TEMPERATURE GRADIENT

Finally, the effects of varying the beam species temperature gradients dn_b/d_r are shown in Fig.9. Again, because of the small beam density fraction and the weak interaction of the beam particles with these roots, the changes in the eigenfrequencies and in the normalized particle and energy fluxes are small for all species, in an absolute sense, but are again substantial in a relative sense for $\Gamma_b T_b/Q_{tot}$ and Q_b/Q_{tot} (though not as large as when varying $dnb=dr$).

6. EXPERIMENTAL COMPARISONS

The TRANSP transport analysis code [21] has been used to derive experimental particle and energy fluxes, from the time evolution of the experimental density and temperature profiles and the particle and energy sources and sinks, for the different plasma species, with some limitations for these cases. The experimentally-derived normalized particle fluxes $\Gamma_j T_j/Q_{tot}$ are all small, as are also the corresponding calculated quasilinear normalized particle fluxes. However, the experimentally-derived fluxes are diffcult to distinguish from zero, within the experimental uncertainties, so only the normalized energy fluxes will be compared quantitatively here. TRANSP can calculate only Q_e and $Q_{therm-ion}$, where $Q_{therm-ion} \equiv Q_i + Q_{Ar} + Q_C$ for the JET case and $Q_{therm-ion} \equiv Q_i + Q_{Ne} + Q_C$ for the NSTX case. The experimentally-derived normalized energy fluxes are $Q_e/Q_{tot} \simeq (1 - Q_{therm-ion}/Q_{tot}) = 0.1$ for the JET case and 0.85 for the NSTX case (Q_b/Q_{tot} is negligable compared to Q_j/Q_{tot} for the other species, for both cases). The corresponding quasilinear normalized energy fluxes are $Q_e/Q_{tot} \simeq (1 - Q_{therm-ion}=Q_{tot}) = 0.2$ for the JET case hybrid root and 0.44 for the NSTX case for the dominant ITG root, for the experimental parameters. Thus, the quasi- linear ratios differ from the corresponding experimentally-derived ratios by about a factor of two for both cases

(but in opposite directions for the two cases). A factor of two disageement is not surprising, considering the approximations in the calculation here. The FULL code calculation is linear and quasilinear (a weak turbulence limit) and is radially local, while the experiments are in some sort of fully-turbulent state and include radially-nonlocal effects as well. In addition, each FULL code calculation only includes a single $k_\theta \rho_i$ value, while the experiments include contributions from a broad spectrum of fluctuations, including possibly much shorter and much longer wavelengths.

GENERAL TRENDS AND CONCLUSIONS

From the results presented in Sec.5, we can draw a number of general conclusions. (i) The range of density and temperature gradient variation surveyed here for the five species often involves regime change, between stable and unstable, or between ITG-like and TEM-like. (ii) Usually, when there are large changes in the gradients, the normalized fluxes $\Gamma_j T_j / Q_{tot}$ and Q_j / Q_{tot} are not linear in the gradients, *i.e.*, the diffusive approximation is not accurate in this situation. Of course, there would be additional gradient dependence in the unnormalized fluxes Γ_j and Q_j due to the gradient dependence of Q_{tot}. (iii) The particle fluxes Γ_j are always small compared to Q_{tot} / Tj , and thus to the largest of the Q_j / T_j. (iv) For all the roots, the strongest overall dependence of the normalized fluxes is on the electron density gradient and the (background thermal deuterium) ion temperature gradient, even for the impurity and beam species. (v) The hot deuterium beam species normalized particle and energy fluxes are also strongly dependent on the beam species density gradient, and to a lesser extent, on the beam species temperature gradient. (vi) The background thermal deuterium ion particle flux is often inwards, to satisfy the condition of ambipolarity discussed in Sec.4. (vii) The other fluxes are usually outward, except occasionally for the small argon or neon fluxes, and occasionally for the small beam fluxes. (viii) Despite the substantial differences between the JET and NSTX experiments, there appear to be many common qualitative trends in the effects of varying individual gradients for these cases, as described in Sec.5.

The breakdown of the "diffusive" approximation was previously investigated in another way in [22] by quantitatively evaluating the power-series coefficient matrices through second order (quadratic in the gradients). This was done in that reference for a simplified case with only three gradients and three fluxes, corresponding to a plasma with only electrons and background hydrogenic ions. It was concluded there that the quadratic contributions to the total fluxes were larger than the linear contributions, *i.e.*, the power series for the case there appeared to be diverging, and not converging. That result is consistent with the present result that the departure of the multispecies fluxes from "linearity" in the gradients is large when the relative change in the normalized fluxes is substantial.

The experimentally-derived normalized electron energy fluxes for the two cases differ by about a factor of two from the corresponding quasilinear normalized electron energy fluxes. This is not surprising, considering the limitations of the calculation employed here. The results presented here are in the linear and quasilinear limit, and are only for a single flux surface and a single value of $k_\theta \rho_i$ for each root, and the behaviour over a wider range in r/a or in $k_\theta \rho_i$ could be different. In the future,

radially-global nonlinear simulations should be able to provide much better calculated information about the density and temperature profile dependence of the flux profiles for each species.

ACKNOWLEDGEMENTS

The authors would like to thank Dr. D. Stutman for providing the input data for the NSTX case, and Dr. Stutman and Dr. T. S. Hahm for useful discussions. The authors would also like to thank the JET and NSTX teams for providing excellent plasmas and data. This work was supported by U.S. DOE Contract No. DE-AC02-76-CHO-3073.

REFERENCES

[1]. G. Rewoldt, W. M. Tang, and M. S. Chance, Phys. Fluids **25**, 480 (1982).

[2]. G. Rewoldt, W. M. Tang, and R. J. Hastie, Phys. Fluids **30**, 807 (1987).

[3]. H. Nordman, J. Weiland, and A. Jarmén, Nucl. Fusion **30**, 983 (1990); J. Weiland and A. Hirose, Nucl. Fusion **32**, 151 (1992); J. Nilsson and J. Weiland, Nucl. Fusion **34**, 803 (1994).

[4]. C. E. Singer, Comments Plasma Phys. Controlled Fusion **11**, 165 (1988).

[5]. G. Bateman, A. H. Kritz, J. E. Kinsey, A. J. Redd, and J. Weiland, Phys. Plasmas **5**, 1793 (1998).

[6]. C. E. Singer, D. E. Post, D. R. Mikkelsen, *et al.*, Comput. Phys. Commun. **49**, 275 (1998).

[7]. M. Kotschenreuther, G. Rewoldt, and W. M. Tang, Comp. Phys. Comm. **88**, 128 (1995).

[8]. W. D. Dorland, F. Jenko, M. Kotschenreuther, and B. N. Rogers, Phys. Rev. Lett. **85**, 5579 (2000).

[9]. J. Candy and R. E. Waltz, J. Comput. Phys. **186**, 545 (2003).

[10]. Z. Lin, T. S. Hahm, W. W. Lee, W. M. Tang, and R. B. White, Science **281**, 1835 (1998).

[11]. A. M. Dimits, G. Bateman, M. A. Beer, *et al.*, Phys. Plasmas **7**, 969 (2000).

[12]. D. R. Ernst, P. T. Bonoli, P. J. Catto, *et al.*, Phys. Plasmas **11**, 2637 (2004).

[13]. P. Helander and D. J. Sigmar, *Collisional Transport in Magnetized Plasmas* (Cambridge University Press, Cambridge, 2002).

[14]. R. Balescu, Phys. Fluids B**4**, 91 (1991).

[15]. T. S. Hahm and W. M . Tang, Phys. Fluids B**3**, 989 (1991).

[16]. P. H. Rebut and B. E. Keen, Fusion Technol. **11**, 13 (1987).

[17]. M. Ono, S. M. Kaye, Y.-K. M. Peng, *et al*, Nucl. Fusion **40**, 557 (2000).

[18]. J. Ongena, P. Monier-Garbet, W. Suttrop, *et al*, Nucl. Fusion **44**, 124 (2004); P. Dumortier, P. Andrew, G. Bonheure, *et al*, Plasma Phys. Control. Fusion **44**, 1845 (2002).

[19]. D. Stutman, M. Finkenthal, R. E. Bell, *et al*, Phys. Plasmas **10**, 4387 (2003).

[20]. J. M. Greene and M. S. Chance, Nucl. Fusion **21**, 453 (1981).

[21]. R. Goldston, *Basic Physical Processes of Toroidal Fusion Plasmas* (Proc. Course and Workshop, Varenna, 1985), Vol. 1, p. 165 (Monotypia Franchi, Cittµa di Castello, 1985).

[22]. See National Technical Information Service Document No. PPPL-2650, by G. Rewoldt (Princeton Plasma Physics Laboratory Report PPPL-2650, 1989).

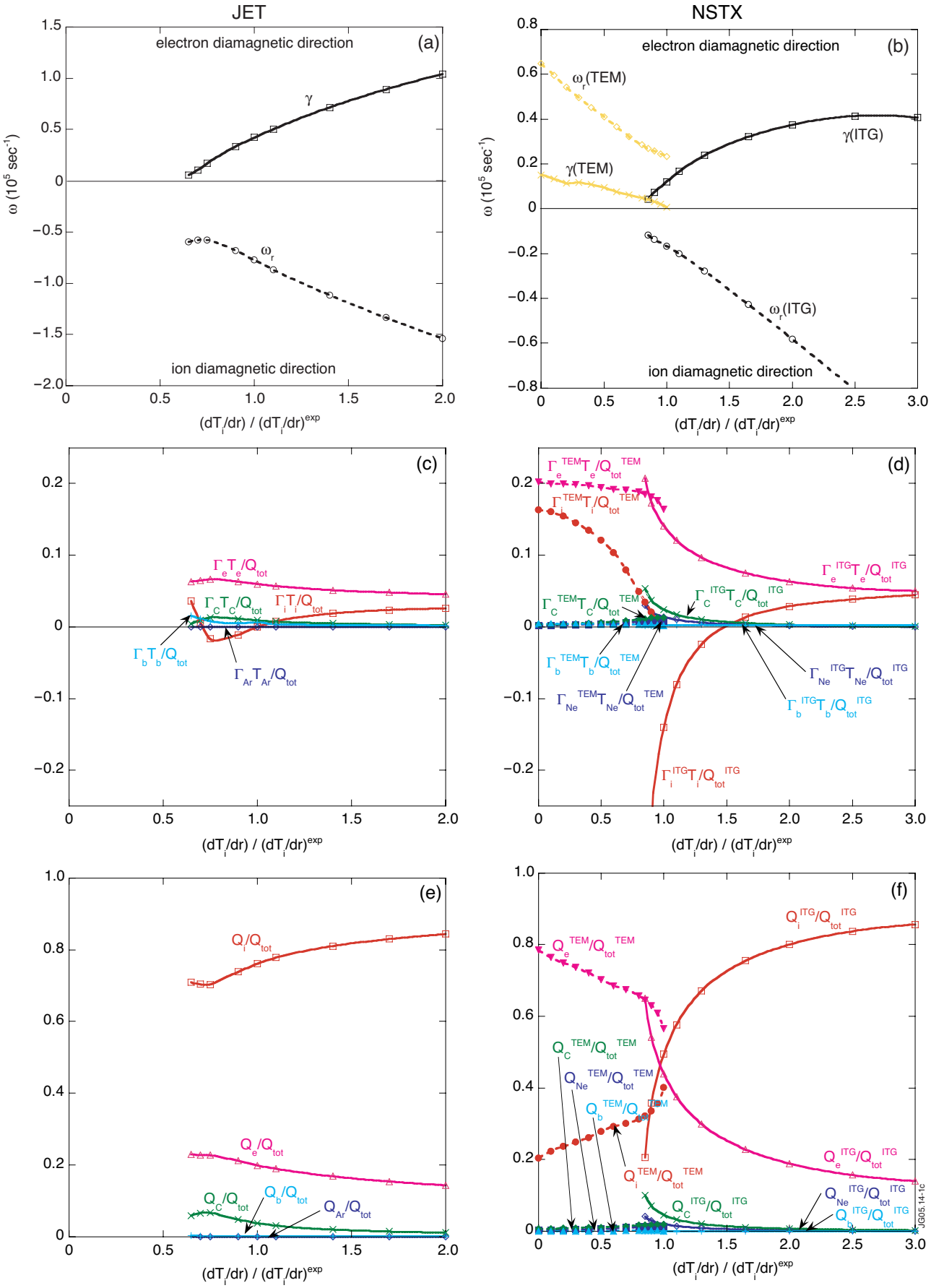

Figure 1: Variation of the growth rate, real frequency, normalized particle fluxes, and normalized energy fluxes with variation of the background thermal deuterium ion temperature gradient.

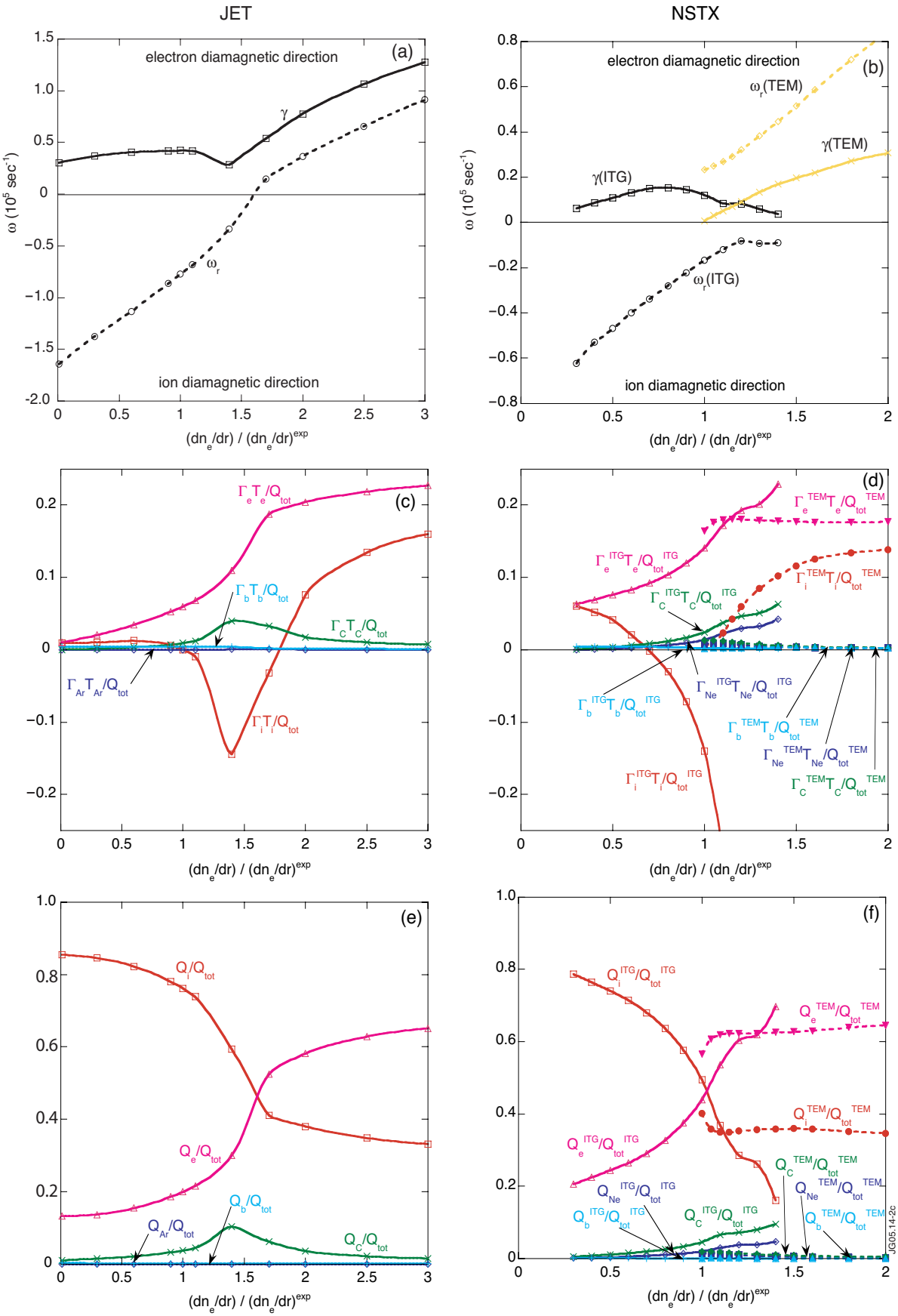

Figure 2: Variation of the growth rate, real frequency, normalized particle fluxes, and normalized energy fluxes with variation of the electron density gradient.

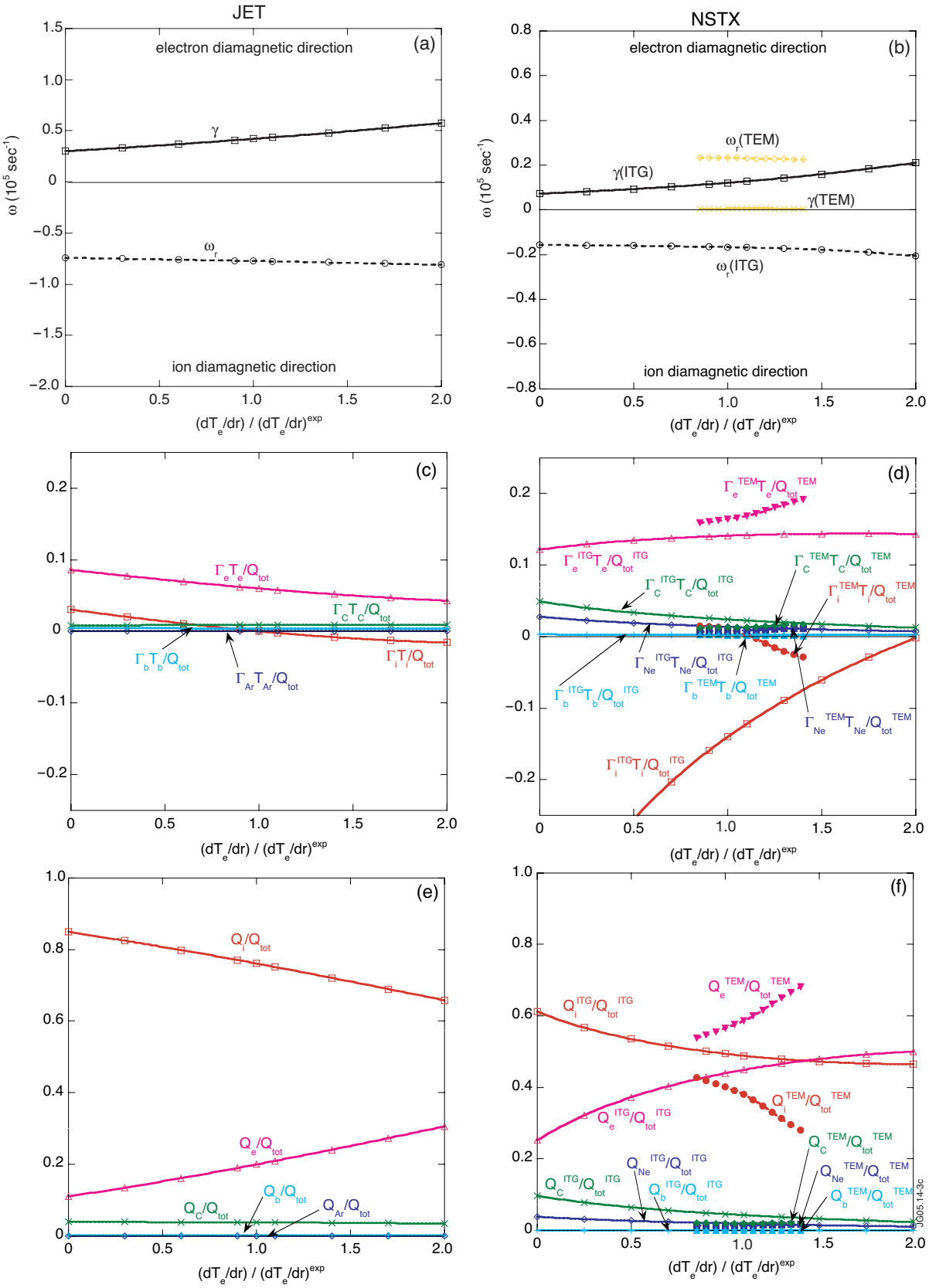

Figure 3: Variation of the growth rate, real frequency, normalized particle fluxes, and normalized energy fluxes with variation of the electron temperature gradient.

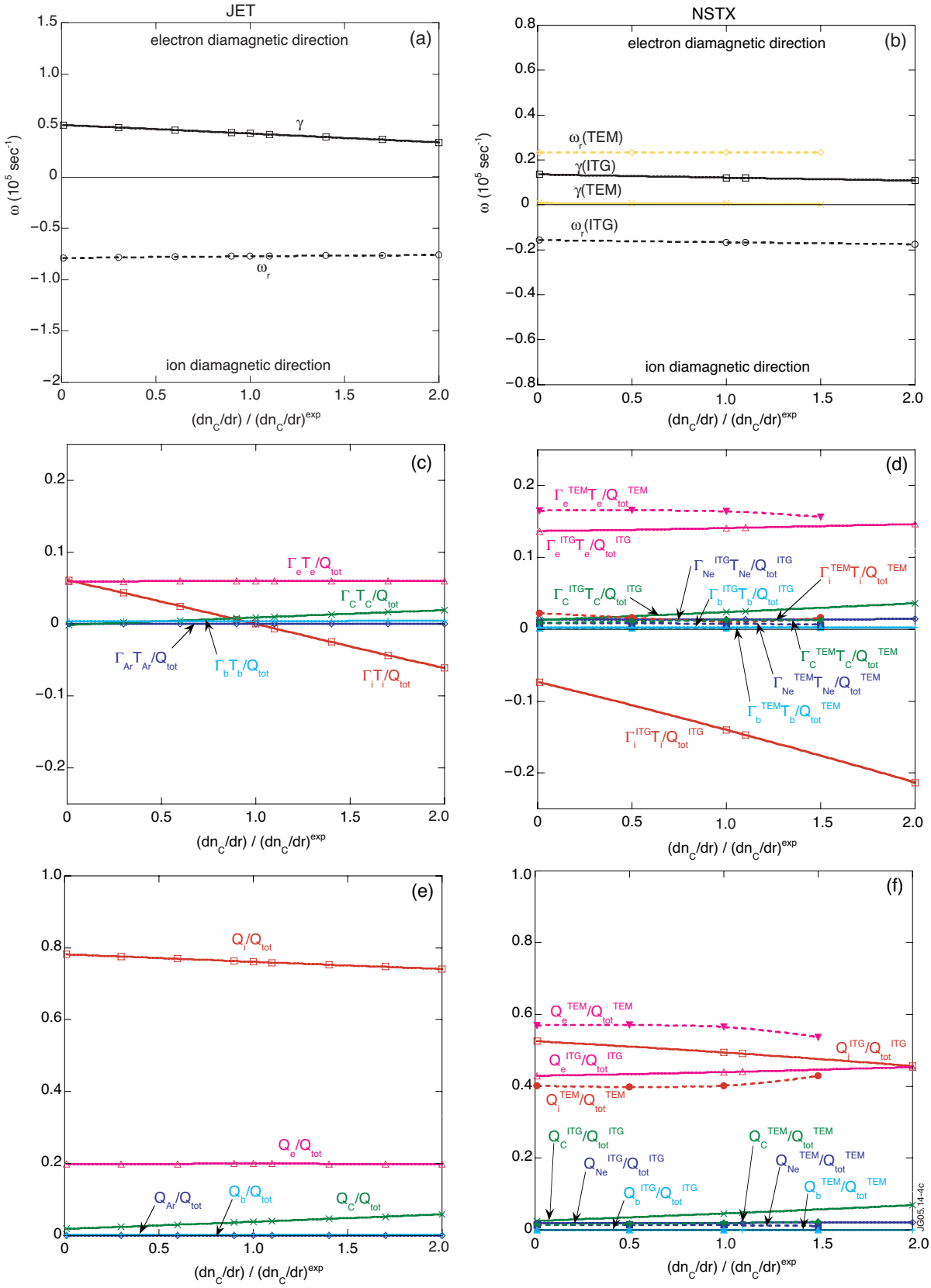

Figure 4: Variation of the growth rate, real frequency, normalized particle fluxes, and normalized energy fluxes with variation of the carbon density gradient.

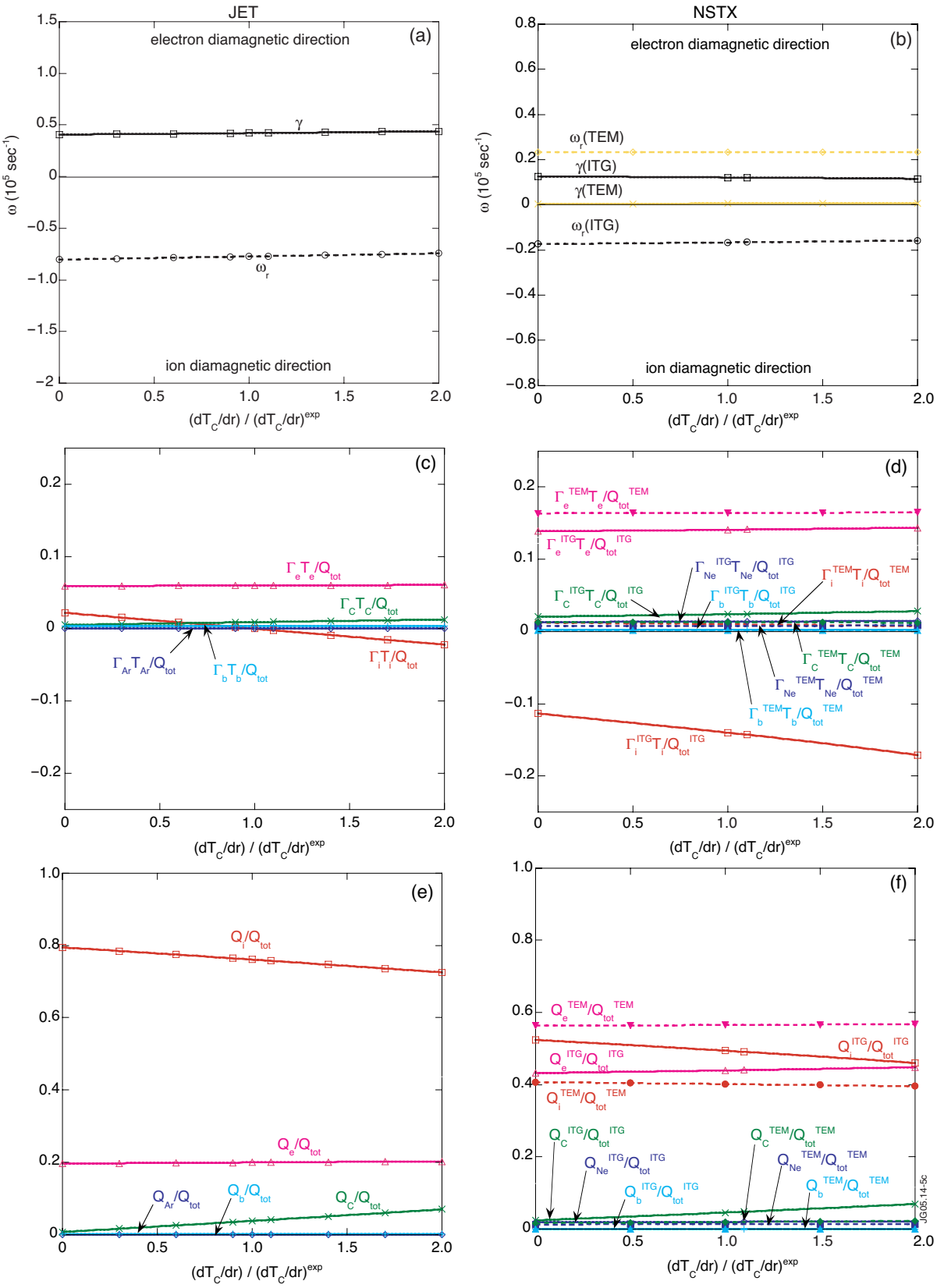

Figure 5: Variation of the growth rate, real frequency, normalized particle fluxes, and normalized energy fluxes with variation of the carbon temperature gradient.

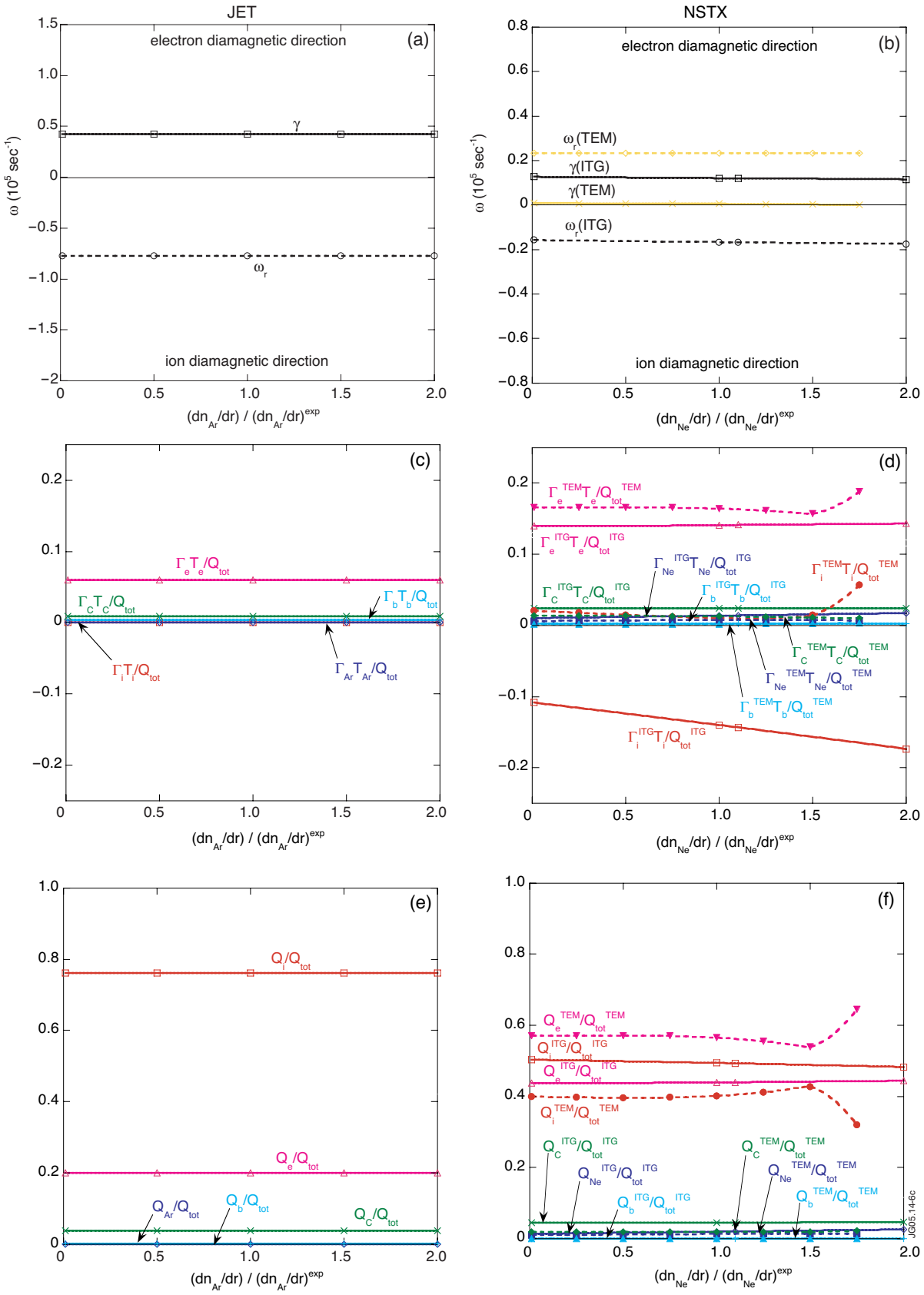

Figure 6: Variation of the growth rate, real frequency, normalized particle fluxes, and normalized energy fluxes with variation of the argon or neon density gradient.

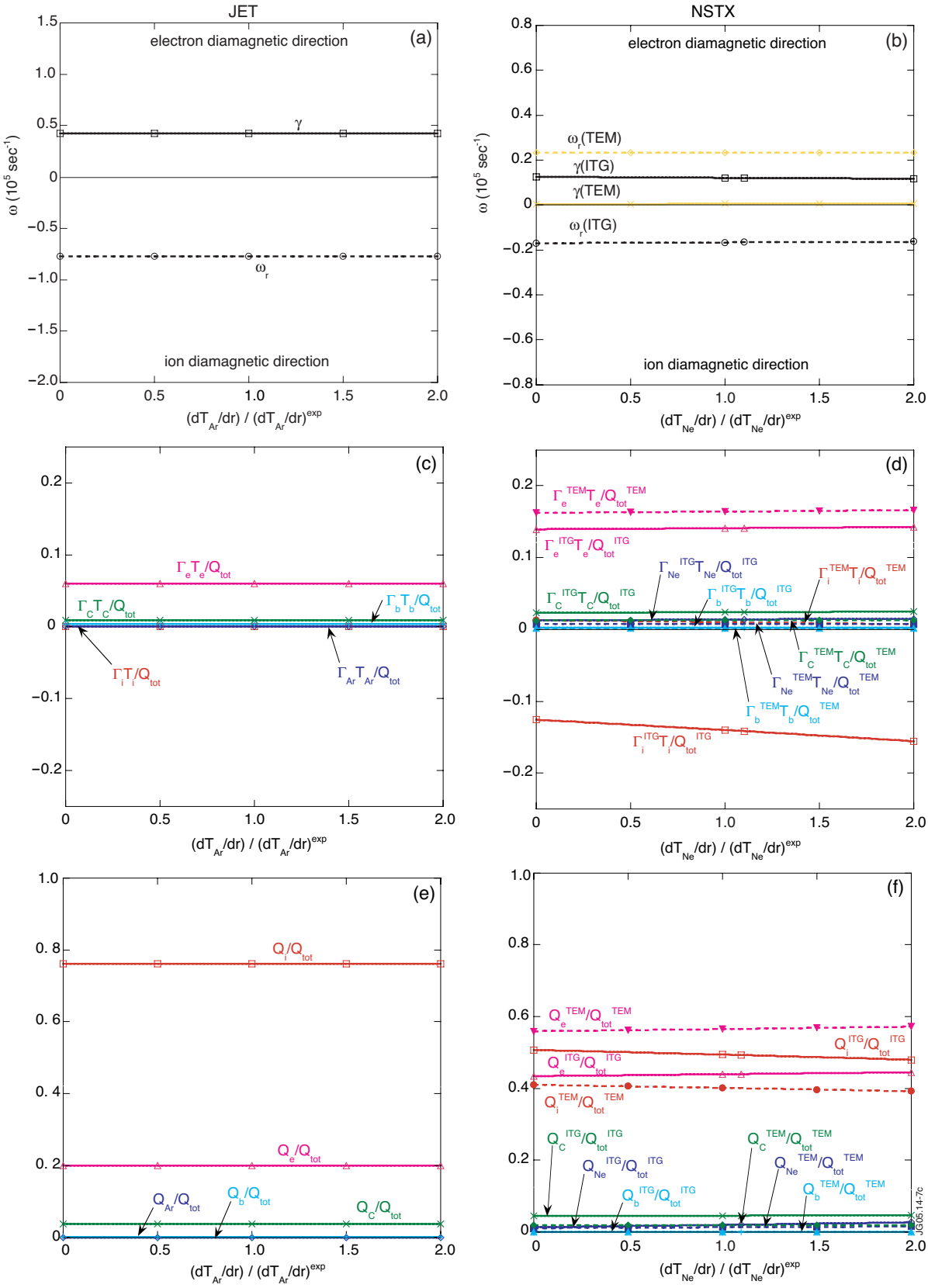

Figure 7: Variation of the growth rate, real frequency, normalized particle fluxes, and normalized energy fluxes with variation of the argon or neon temperature gradient.

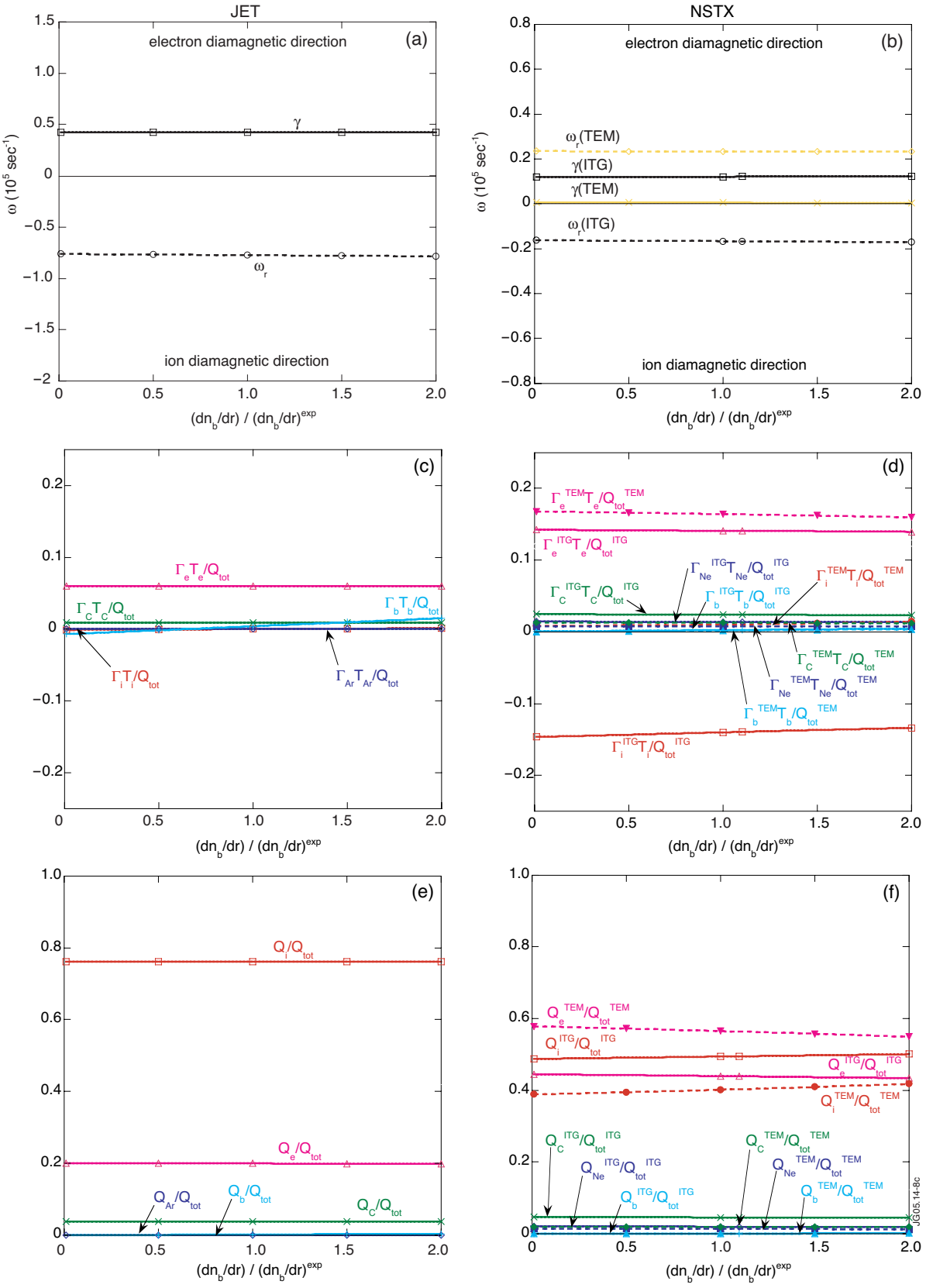

Figure 8: Variation of the growth rate, real frequency, normalized particle fluxes, and normalized energy fluxes with variation of the hot deuterium beam density gradient.

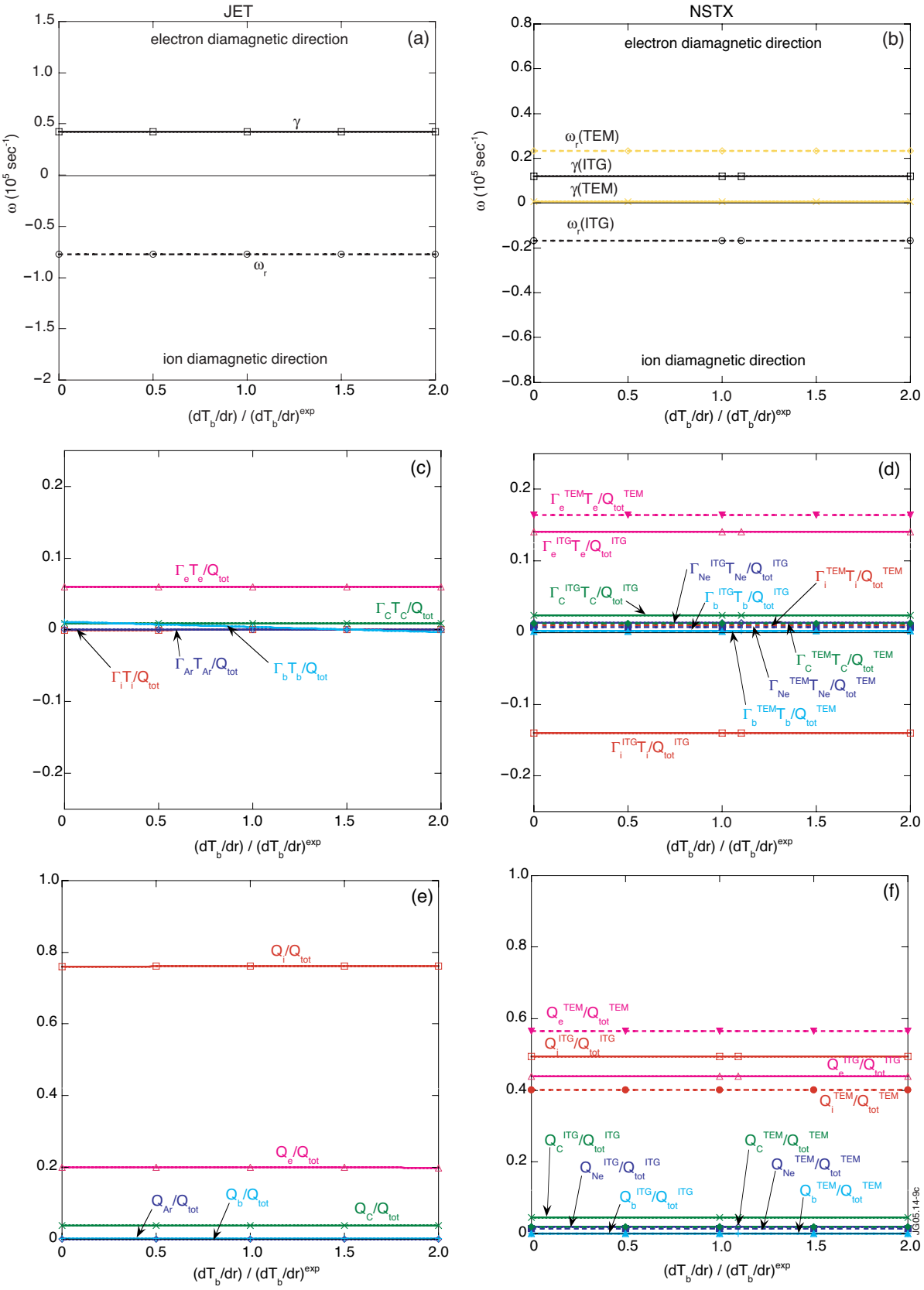

Figure 9: Variation of the growth rate, real frequency, normalized particle fluxes, and normalized energy fluxes with variation of the hot deuterium beam temperature gradient